Reprinted from TEMPERATURE—ITS MEASUREMENT AND CONTROL IN SCIENCE AND INDUSTRY, Vol. 3, Part 1

56. Spectroscopic Methods of Temperature Measurements*

S. S. PENNER

Daniel and Florence Guggenheim Jet Propulsion Center, California Institute of Technology, Pasadena, Calif.

Spectroscopic methods for temperature measments have been described in previous volumes of this series,[1, 2] as well as in a number of recently published books.[3-5] Among the well-recognized procedures for temperature determinations, we note the following: measurements of brightness temperatures, color temperatures, and reversal temperatures; multiple-path procedures for temperature determinations; population temperature estimates; direct measurements of translational temperatures from spectral line profiles; temperature measurements from the intensity profiles of continuum radiation in ionized gases; temperature measurements from spectral line shifts in ionized gases; etc.

Because many interesting physical phenomena are being studied in systems in which (nearly) isothermal conditions are maintained for very short periods of time, considerable effort has been devoted recently to the development of measurement techniques that can be used in times of the order of 10^{-3} to 10^{-6} second. Examples of these studies are measurements behind shock fronts of sodium line reversal temperatures;[6, 7] time-dependent color temperature measurements behind carbon-producing shocks;[8] direct population temperature determinations from spectrographic records on very intense radiators by using a rotating-drum camera[9, 10] spectrograph; temperature measurements on highly ionized gases using Stark line profiles;[10] population temperature measurements behind shock fronts using two fairly narrow wavelength regions and a suitable filter or spectrograph; and line shift determinations in highly ionized gases.[9]

Important recent contributions to the spectroscopic procedures for temperature determinations include the development of techniques for constructing temperature profiles in axially symmetric systems such as plasmas, shock tubes, and rocket exhaust flows.[11]

* Supported by the Office of Scientific Research, U.S. Air Force, under Contract AF 49(638)-984.

ABSORPTION-EMISSION PYROMETRY

Equilibrium Temperature Measurements with High Time Resolution

Among the most widely used optical procedures for temperature determinations are the line (or band) reversal techniques. It is well-known and easily demonstrated that, at the point of reversal, the temperature of an absorbing and emitting gas region equals the brightness temperature of the comparison source.*

Temperature measurements of heated gases can be performed with high time resolution by using multiple-path procedures provided the emitting region is neither optically thin nor black.*

For heated gases we must generally perform two measurements in order to determine the two unknown quantities that determine the absorptive and emissive properties of heated gases, *viz.*, the spectral emissivities and the local temperature. Although the general principles involved in absorption-emission pyrometry have been understood for more than half a century, this technique

* See, for example, Chap. 16 in reference 3.

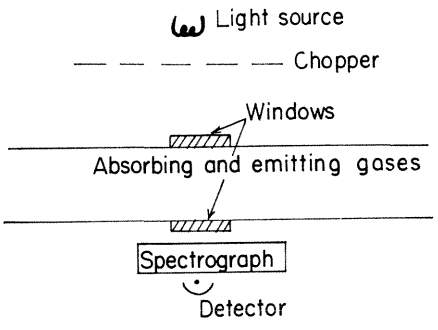

FIG. 1. Schematic diagram showing the principal components used in Silverman's application of absorption-emission pyrometry.

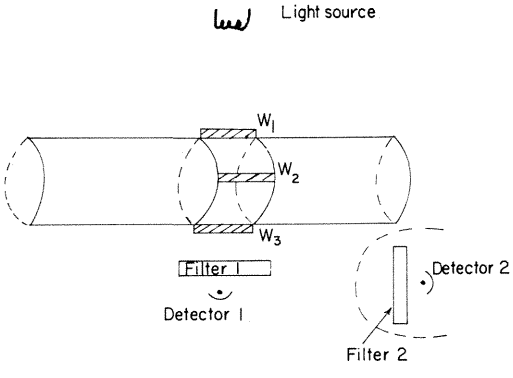

FIG. 2. Schematic diagram showing a suitable experimental arrangement for high-speed absorption-emission pyrometry on gases. The window W_2 permits observations in a direction normal to that made with detector 1; detector 2 is located in such a way that it may be used to measure flux densities in the direction normal to the plane of the paper.

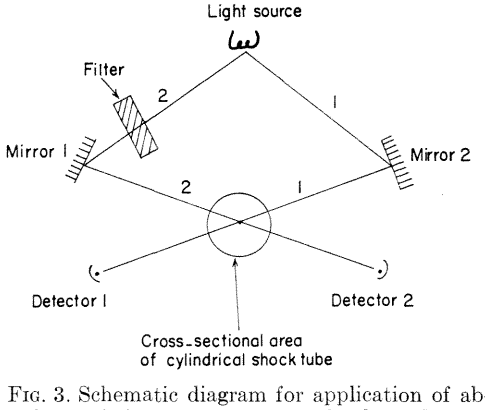

FIG. 3. Schematic diagram for application of absorption-emission pyrometry to the heated gases located in a plane behind a shock front.

has been revived in modified form in recent years because the development of new experimental facilities has permitted the introduction of useful variants of earlier applications. The form in which the method was applied by Silverman[12, 3] is shown in the schematic diagram of Fig. 1. The gas temperature is determined by considering the quantitative significance of the observed spectral radiant flux densities originating (a) from the light source, (b) from the emitting gases, and (c) from the light source as viewed through the emitting gases. The last-mentioned measurement is made possible by using a chopper and suitable amplifier in order to discriminate between the gas and source radiation. This technique can be applied with a time resolution of the order of a few microseconds by employing a high-speed mechanical chopper mounted on a helium-driven turbine, which permits the attainment of repetition rates of the order of 0.1 microsecond; with air-driven turbines, a repetition rate of 1 microsecond is feasible.[13] For work in the infrared regions of the spectrum, it is necessary to utilize photoconductive receivers such as a gold-doped Ge cell (response times of the order of a few tenths of a microsecond).

For still greater time resolution, the schematic arrangement sketched in Fig. 2 may be used. The temperature is now determined from data on the direct measurement of the flux densities originating from (a) the source alone, (b) the heated gases alone, and (c) the heated gases and source viewed together. The experimental arrangement sketched in Fig. 2 has the disadvantage of requiring a calibration of the two detectors relative to each other. In practice, this calibration may be performed conveniently by matching the output produced by the two detectors and their respective amplifying circuits for the same source, namely, for the heated gases.

A variation of the technique of absorption-emission pyrometry that is related to a procedure which Gaydon has employed recently in measurements on shock tubes[6, 7] is sketeched in Fig. 3. We shall illustrate the interpretation of the experimental data by performing a complete analysis of the following measured spectral steradiancies: (a) the apparent spectral steradiancy of the source $B_{\nu,1}$ at the frequency ν without absorption or emission in the shock tube; (b) the apparent spectral steradiancy of the source viewed through a filter $B_{\nu,2}$ without absorption or emission in the shock tube; (c) the corresponding steradiancies $B'_{\nu,1}$ and $B'_{\nu,2}$ that are observed when the heated gases in the shock tube absorb and emit radiant energy.

Time-resolved data can be obtained across the field of view with the attainable time resolution determined by the response characteristics of the detectors and associated amplifying circuits.

The phototube output signals after amplification are adjusted to be identical when the filter F is removed. We assume linearity between signals and incident steradiancies after the matching of outputs has been accomplished. The following relations apply:

$$B_{\nu,1} = \epsilon_{\nu,s} B^0_{\nu,s} \tag{1}$$

$$B_{\nu,2} = \epsilon_{\nu,s} B^0_{\nu,s}(1 - \alpha_{\nu,F}) \tag{2}$$

$$\begin{aligned} B'_{\nu,1} &= \epsilon_{\nu,s} B^0_{\nu,s}(1 - \alpha_{\nu,g}) + \epsilon_{\nu,g} B^0_{\nu,g} \\ &= B_{\nu,1}(1 - \alpha_{\nu,g}) + \epsilon_{\nu,g} B^0_{\nu,g} \end{aligned} \tag{3}$$

$$\begin{aligned} B'_{\nu,2} &= \epsilon_{\nu,s} B^0_{\nu,s}(1 - \alpha_{\nu,F})(1 - \alpha_{\nu,g}) + \epsilon_{\nu,g} B^0_{\nu,g} \\ &= B_{\nu,2}(1 - \alpha_{\nu,g}) + \epsilon_{\nu,g} B^0_{\nu,g} \end{aligned} \tag{4}$$

Here ϵ_ν and α_ν denote spectral emissivities and absorptivities, respectively, the superscript 0 identifies blackbody properties, and the subscripts s, F, and g identify source, filter, and gas properties, respectively. But, it follows from Kirchhoff's law that

$$\alpha_{\nu,g} = \epsilon_{\nu,g}$$

whence

$$B'_{\nu,1} = B_{\nu,1} + \epsilon_{\nu,g}(B^0_{\nu,g} - B_{\nu,1})$$

$$B'_{\nu,2} = B_{\nu,2} + \epsilon_{\nu,g}(B^0_{\nu,g} - B_{\nu,2})$$

and

$$\epsilon_{\nu,g} = \frac{B'_{\nu,1} - B_{\nu,1}}{B^0_{\nu,g} - B_{\nu,1}} = \frac{B'_{\nu,2} - B_{\nu,2}}{B^0_{\nu,g} - B_{\nu,2}} \tag{5}$$

Also

$$\begin{aligned} B^0_{\nu,g} &= B_{\nu,1} + \frac{1}{\epsilon_{\nu,g}}(B'_{\nu,1} - B_{\nu,1}) \\ &= B_{\nu,2} + \frac{1}{\epsilon_{\nu,g}}(B'_{\nu,2} - B_{\nu,2}) \\ &= B_{\nu,1} + (B^0_{\nu,g} - B_{\nu,2})\frac{B'_{\nu,1} - B_{\nu,1}}{B'_{\nu,2} - B_{\nu,2}} \end{aligned}$$

or

$$B^0_{\nu,g}\left(1 - \frac{B'_{\nu,1} - B_{\nu,1}}{B'_{\nu,2} - B_{\nu,2}}\right) = B_{\nu,1} - B_{\nu,2}\frac{B'_{\nu,1} - B_{\nu,1}}{B'_{\nu,2} - B_{\nu,2}}$$

or

$$\frac{B^0_{\nu,g}}{B_{\nu,1}} = \frac{(B'_{\nu,2} - B_{\nu,2}) - (B_{\nu,2}/B_{\nu,1})(B'_{\nu,1} - B_{\nu,1})}{(B'_{\nu,2} - B_{\nu,2}) - (B'_{\nu,1} - B_{\nu,1})} \tag{6}$$

Equation (6) has been used[6, 7] for the special case in which the source temperature and filter were chosen in such a way that

$$B'_{\nu,1} < B_{\nu,1} \quad \text{and} \quad B'_{\nu,2} > B_{\nu,2}$$

This restriction is, however, unnecessary.

For

$$B'_{\nu,1} = B'_{\nu,2} = B_{\nu,1} = B_{\nu,2}$$

Eq. (6) becomes indeterminate; for

$$B'_{\nu,2} = B_{\nu,2}\,, \qquad B^0_{\nu,g} = B_{\nu,2};$$

for

$$B'_{\nu,1} = B_{\nu,1}\,, \qquad B^0_{\nu,g} = B_{\nu,1}\,.$$

The two preceding special cases correspond to the conditions satisfied in conventional determinations of reversal temperatures.

In terms of temperatures, Eq. (6) may be written in the following convenient form:

$$\frac{\exp(h\nu/kT_{Br,1}) - 1}{\exp(h\nu/kT_g) - 1} = r \tag{7}$$

where $T_{Br,1}$ is the brightness temperature of the source at the frequency ν, T_g represents the true gas temperature, and

$$r = \frac{(B'_{\nu,2} - B_{\nu,2}) - (B_{\nu,2}/B_{\nu,1})(B'_{\nu,1} - B_{\nu,1})}{(B'_{\nu,2} - B_{\nu,2}) - (B'_{\nu,1} - B_{\nu,1})} \tag{8}$$

is determined directly from the measured steradiancies. Equation (7) may be solved explicitly for T_g with the result

$$T_g = \frac{h\nu}{k \ln (1/r)[\exp(h\nu/kT_{Br,1}) - 1 + r]} \tag{9}$$

or, for $\exp(h\nu/kT_{Br,1}) \gg 1$, $\exp(h\nu/kT_g) \gg 1$,

$$\frac{T_g}{T_{Br,1}} = \frac{1}{1 - (kT_{Br,1}/h\nu)\ln r} \tag{9a}$$

Equation (9) or (9a) may then be used in practice for the determination of T_g from the measured steradiancy ratios and the known value of $T_{Br,1}$.

Measurement of Total Reversal Temperatures*

We define the total reversal temperature as the temperature at which the reversal condition is

* The following discussion is based on an unpublished analysis prepared by the author in collaboration with Dr. U. P. Oppenheim during 1958. The time resolution attainable in measure-

satisfied when observations are made with a black or gray comparison source and the received flux densities are integrated over all wavelengths.

It has been shown[14, 15] that total isothermal gas absorptivities α_{ab} and emissivities ϵ_g are related through expressions of the form

$$\alpha_{ab}(T_s \rightarrow T_g, X) = \left(\frac{T_g}{T_s}\right)^{\beta-1} \epsilon_g\left[T_s, X\left(\frac{T_s}{T_g}\right)^{\beta}; a_{T_g}\right] \quad (10)$$

where T_g is the gas temperature, T_s represents the temperature of a black or gray source used to perform (wavelength integrated) absorptivity measurements, X denotes the optical depth of the gases at T_g, the parameter β depends on the particular band model used to describe the vibration-rotation bands of the gases, and a_{T_g} identifies a line shape parameter at the temperature T_g which measures the relative importance of collision and Doppler broadening. It is apparent that Eq. (10) leads to the condition derivable from Kirchhoff's law that

$$\alpha_{ab} = \epsilon_g \quad \text{at} \quad T_s = T_g \quad (11)$$

for all band models. The validity of Eq. (11) permits a direct experimental determination of the total reversal temperature T_g through the relation

$$\sigma T_s^4 = \sigma T_s^4(1 - \alpha_{ab}) + \epsilon_g \sigma T_g^4 \quad (12)$$

where σ denotes the Stefan-Boltzmann constant. Comparison of Eqs. (11) and (12) shows that $T_g = T_s$ when the blackbody source appears to be equally intense with and without heated gases in the light path.

In practice we have used a gray comparison source and an apparatus that was developed for the direct determination of total absorptivities.[16] A light chopper was located between the absorption cell and the detector (thermopile). In the experimental studies, a gray source of emissivity $\epsilon_s \simeq 0.75$ was used. The ratio $\mathfrak{R}$ of the apparent intensity with the gases in the light path to the intensity of the source alone, *viz.*,

$$\mathfrak{R} = \frac{A\epsilon_s\sigma T_s^4 (1 - \alpha_{ab}) + B\epsilon_g\sigma T_g^4}{A\epsilon_s\sigma T_s^4} \quad (13)$$

was measured for fixed values of T_g and selected values of T_s. In Eq. (13), the parameters A and B are constants depending on geometrical factors which may be made equal by using a suitable instrumental arrangement. Thus Eq. (13) reduces to

$$\mathfrak{R} = (1 - \alpha_{ab}) + \left(\frac{\epsilon_g}{\epsilon_s}\right)\left(\frac{T_g}{T_s}\right)^4 \quad (14)$$

where, however, $\alpha_{ab} \neq \epsilon_g$ and $T_s \neq T_g$ for $\mathfrak{R} = 1$ when $\epsilon_s \neq 1$. In fact,

$$\frac{T_g}{T_s} = \left(\frac{\alpha_{ab}}{\epsilon_g}\epsilon_s\right)^{1/4} \quad \text{for} \quad \mathfrak{R} = 1 \quad (15)$$

But*

$$\frac{\alpha_{ab}}{\epsilon_g} = \left(\frac{T_g}{T_s}\right)^{\beta-1} \quad (16)$$

for $T_g \simeq T_s$ with $\beta = 0$ for transparent gases;[15] Eq. (16) was actually derived for a black source but is easily seen to remain equally valid for a gray source. From Eqs. (15) and (16) we find that

$$\frac{T_g}{T_s} \simeq (\epsilon_s)^{1/(5-\beta)} \quad \text{for} \quad \mathfrak{R} = 1 \quad (17)$$

i.e., the ratio T_g/T_s should decrease from $(\epsilon_s)^{1/5}$ for transparent gases to $(\epsilon_s)^{1/(5-\beta)}$ for large optical depths. We except that $\beta = 0$ for a fairly wide range of conditions since gas absorptivities and emissivities at elevated temperatures are usually small compared to unity.

Representative plots of $\mathfrak{R}$ as a function of T_s are shown in Figs. 4 and 5 for CO_2 and CO, respectively. These molecules have completely different band models. Reference to Figs. 4 and 5 shows that $T_g/T_s \simeq (0.75)^{1/5} = 0.944$ at $\mathfrak{R} = 1$ in accord with the transparent gas expression obtained from Eq. (17) for $\beta = 0$.

MEASUREMENT OF POPULATION TEMPERATURES

The principles and assumptions involved in population temperature measurements have been discussed exhaustively[2, 3] in a number of previously published articles and need not be reexamined in the present survey. There are, how-

ments of total reversal temperature is severely limited by the nonexistence of very fast black receivers. With available facilities, it is probably not feasible to obtain response times shorter than 10^{-2} to 10^{-3} second.

* We assume here that the variation of the emissivity is negligibly small in the temperature interval $T_g \leq T \leq T_s$. This assumption is reasonably well satisfied for the particular gases and temperatures chosen in our experimental studies.

ever, some interesting peculiarities involved in population temperature measurements with high time resolution of emitters behind shock fronts when the optical system is arranged in such a way that the detector responds to the radiant energy emitted from a group of spectral lines belonging to a band or band system of a specified emitter. We shall restrict our discussion of population temperature measurements to this special case.

Population Temperature Estimates from Determinations of Absolute Emission Intensities

Population temperature measurements on emitters with nonoverlapping spectral lines can be performed if independent absolute intensity and concentration estimates are available. This technique may be used, for example, on OH behind shock fronts, in which case the principal source of error is associated with the uncertainties in the f number for the emitting species and in uncertainties concerning the gas composition, which is a unique function of the temperature only if equilibrium obtains. Available experimental data[17] on OH show, for example, that the equilibrium gas composition is reached in times of the order of 30 microseconds for OH formed from H_2O in Ar containing about 1% of H_2O at temperatures close to 4000°K. Hence the requirements for a significant temperature measurement may well be satisfied for this emitter in many interesting shock-tube experiments. Temperature determinations from absolute emission intensities for OH require essentially the same experimental procedure that was used for a redetermination of the f number of OH for the (0, 0) band, $^2\Sigma \longrightarrow {}^2\Pi$ transitions.[17] The complete program involves independent successive measurements of (1) the instrumental slit function, (2) the emission intensity from the shocked gases, and (3) an absolute calibration experiment.

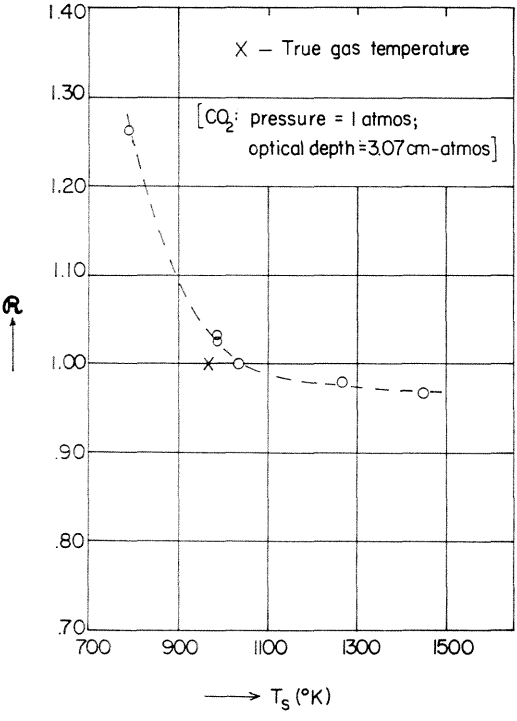

FIG. 4. The ratio $\mathcal{R}$ as a function of T_s for CO_2 at atmospheric pressure, $X = 3.07$ cm-atmos, $T_g = 966$°K.

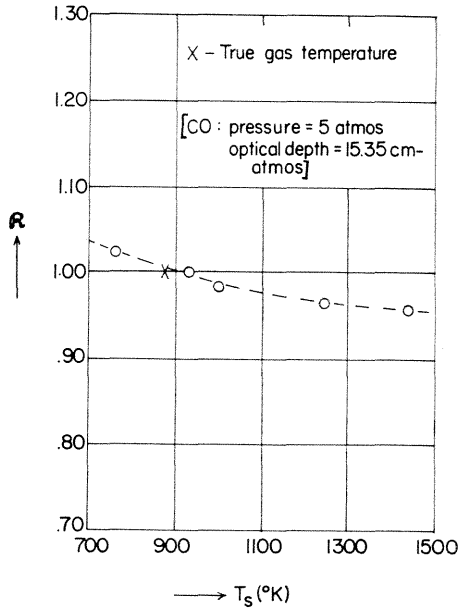

FIG. 5. The ratio $\mathcal{R}$ as a function of T_s for CO at a pressure of 5 atmos, $X = 15.35$ cm-atmos, $T_g = 875$°K.

Let $g(|\omega' - \omega|; b', c')$ be a dimensionless slit function for the instrument used in the experimental studies.* This slit function measures the instrumental response at ω' when the instrument is set at ω; b' and c' are instrumental parameters that are presumably independent of the particular instrumental setting. The slit function is conveniently normalized in such a way that

$$\frac{\int_{\omega-\Delta\omega^*}^{\omega+\Delta\omega^*} g(|\omega' - \omega|; b', c')\, d\omega'}{\Delta\omega^*} = 1$$

* Cf. Chap. 5 of reference 3.

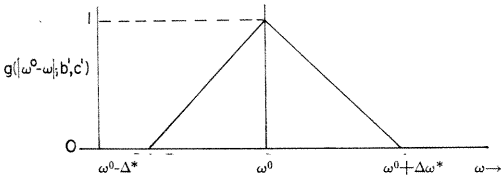

FIG. 6. Schematic diagram showing the variation of the slit function $g(|\omega^\circ - \omega|;b',c')$ with wave number for a typical prism instrument.

where $g(0; b', c') = 1$ and $g(|\omega' - \omega|; b', c') = 0$ for $|\omega' - \omega| \geq \Delta\omega^*$. The slit function is determined in the usual way by making observations with a sufficiently narrow source. The apparent spectral source flux density $(2\Delta\omega^* I^a_{s,\omega})$ integrated over the slit width $2\Delta\omega^*$ when the instrument is set at ω, for a source emitting $I_{s,\omega'}$ ergs/cm²-sec-cm^{-1}, in the wave-number interval between ω' and $\omega' + d\omega'$, is

$$2\Delta\omega^* I^a_{s,\omega} = \int_{\omega-\Delta\omega^*}^{\omega+\Delta\omega^*} I_{s,\omega'} g(|\omega' - \omega|; b', c')\, d\omega'$$

If the source acts like a delta function and emits the total flux density I_s (ergs/cm²-sec) at

$$\omega' = \omega^0 \left[\text{i.e., } I_s = \int_{-\infty}^{\infty} I_{s,\omega'}\, d(\omega' - \omega^0)\right],$$

then

$$2\Delta\omega^* I^a_{s,\omega} = g(|\omega^0 - \omega|; b', c') I_s$$

Also

$$2\Delta\omega^* I^a_{s,\omega^0} = I_s$$

since we have chosen to normalize g in such a way that $g(0; b', c') = 1$. Hence it follows that the slit function

$$g(|\omega^0 - \omega|; b', c') = I^a_{s,\omega}(2\Delta\omega^*)/I^a_{s,\omega^0}(2\Delta\omega^*) \tag{18}$$

may be determined directly by measuring simply the ratio of the apparent flux density at ω to the apparent flux density at ω^0. For a prism instrument, $g(|\omega^0 - \omega|; b', c')$ is expected to represent the triangular slit function sketched in Fig. 6, which has the previously specified normalization properties.

Let $S^a_{L,i}$(cm^{-2}-atoms^{-1}) denote the apparent integrated intensity of the ith isolated spectral line falling in the wave-number interval $\omega_0 - \Delta\omega^* \leq \omega \leq \omega_0 + \Delta\omega^*$ where ω_0 need not coincide with the location of the calibration line at ω^0 but where it should, nevertheless, be justified to assume that $g(|\omega_0 - \omega|; b', c')$ has the same shape in the vincinity of ω_0 as has $g(|\omega^0 - \omega|; b', c')$ near ω^0. The optical depth of the emitting species is X (cm-atmos), and the true spectral absorption coefficient is $P_{L,i,\omega}$ for the ith spectral line. The apparent observed steradiancy for transparent gases when the instrument is set at ω_0 becomes now

$$\begin{aligned}\frac{X}{\pi}\sum_i R^0_{\omega_i} S^a_{L,i} &= \frac{1}{\pi}\sum_i \int_{\omega_0-\Delta\omega^*}^{\omega_0+\Delta\omega^*} R^0_{\omega_i}[1 - \exp(-P_{L,i,\omega}X)] \\ &\qquad \cdot g(|\omega_0 - \omega|; b', c')\, d\omega' \\ &\simeq \frac{X}{\pi}\sum_i \int_{\omega_0-\Delta\omega^*}^{\omega_0+\Delta\omega^*} R^0_{\omega_i} P_{L,i,\omega} g(|\omega_0 - \omega|; b', c')\, d\omega\end{aligned} \tag{19}$$

where $R^0_{\omega_i}$ is the spectral blackbody radiancy at ω_i. If $2\Delta\omega^*$ is sufficiently small, then we may approximate all of the $R^0_{\omega_i}$ by $R^0_{\omega_0}$; furthermore, if the spectral lines are sufficiently narrow, then

$$\int_{\omega_0-\Delta\omega^*}^{\omega_0+\Delta\omega^*} P_{L,i,\omega} g(|\omega_0 - \omega|; b', c')\, d\omega \simeq g(|\omega_0 - \omega_i|; b', c') S_{L,i}$$

Hence

$$\frac{X}{\pi}\sum_i R^0_{\omega_i} S^a_{L,i} \simeq \frac{X}{\pi}\sum_i R^0_{\omega_i} g(|\omega_0 - \omega_i|; b', c') S_{L,i} \tag{20}$$

or

$$\frac{X}{\pi} R^0_{\omega_0} \sum_i S^a_{L,i} \simeq \frac{X}{\pi} R^0_{\omega_0} \sum_i g(|\omega_0 - \omega_i|; b', c') S_{L,i} \tag{20a}$$

In the calibration experiment, let a continuous source with spectral emissivity ϵ_ω produce the actual incident flux density

$$\frac{R_s}{\pi} = \int_{\omega_0-\Delta\omega^*}^{\omega_0+\Delta\omega^*} \epsilon_{s,\omega}(R^0_{s,\omega}/\pi)\, d\omega$$

when the instrument is set at the wave number ω_0; the apparent incident flux density is then

$$\frac{R^a_s}{\pi} = \int_{\omega_0-\Delta\omega^*}^{\omega_0+\Delta\omega^*} \epsilon_{s,\omega}\left(\frac{R^0_{s,\omega}}{\pi}\right) \cdot g(|\omega - \omega_0|; b', c')\, d\omega \tag{21}$$

We have already assumed that $R^0_{s,\omega} \simeq R^0_{s,\omega_0}$;

if $\epsilon_{s,\omega} \simeq \epsilon_{s,\omega_0}$, i.e., if the source emissivity is also a slowly varying function of ω, then

$$\frac{R_s^a}{\pi} \simeq \epsilon_{s,\omega_0} \frac{R^0_{s,\omega_0}}{\pi} \Delta\omega^*$$

Hence

$$\frac{\frac{X}{\pi}\sum_i R^0_{\omega_i} S^a_{L,i}}{\frac{R_s^a}{\pi}} \simeq \frac{X}{\pi} \frac{\sum_i R^0_{\omega_i} g(|\,\omega_0 - \omega_i\,|\,;b',c')S_{L,i}}{\int_{\omega_0-\Delta\omega^*}^{\omega_0+\Delta\omega^*} \epsilon_{s,\omega}\left(\frac{R^0_{s,\omega}}{\pi}\right) g(|\,\omega - \omega_0\,|\,;b',c')\,d\omega} \tag{22}$$

or

$$\frac{[(X/\pi)R^0_{\omega_0}]\sum_i S^a_{L,i}}{(R_s^a/\pi)} \simeq \frac{R^0_{\omega_0}X}{\epsilon_{s,\omega_0}R^0_{s,\omega_0}} \frac{\sum_i g(|\,\omega_0 - \omega_i\,|\,;b',c')S_{L,i}}{\Delta\omega^*}, \tag{22a}$$

i.e., a direct measurement of the apparent flux density ratio of the emitting gas to the standard comparison source, for known values of R^0_{s,ω_0}, $\Delta\omega^*$ and $g(|\,\omega_0 - \omega_i\,|\,;b',c')$, permits a unique determination of the temperature since the temperature-dependent factors $X(T)$, $R^0_{\omega_0}(T)$, and $S_{L,i}(T)$ may be computed as functions of the temperature if equilibrium obtains.

Population Temperature Determinations Based on the Measurement of Relative Flux Densities in Two Spectral Regions

The difficult absolute intensity calibration that is implicit in the use of Eqs. (22) and (22a) may be avoided if simultaneous flux density determinations are carried out in two different spectral regions. Thus consider two spectral regions identified by the subscripts i and j, respectively. Then the ratio ot the measured apparent flux densities

$$\frac{\sum_i R^0_{\omega_i} S^a_{L,i}}{\sum_j R^0_{\omega_j} S^a_{L,j}}$$

becomes a known calculable function of the temperature. Using Eq. (22), we find that

$$\frac{\sum_i R^0_{\omega_i} S^a_{L,i}}{\sum_j R^0_{\omega_j} S^a_{L,j}} = \frac{\sum_i R^0_{\omega_i} g(|\,\omega_i - \omega_{0i}\,|\,;b',c')S_{L,i}}{\sum_j R^0_{\omega_j} g(|\,\omega_j - \omega_{0j}\,|\,;b',c')S_{L,j}} \equiv \varphi(T) \tag{23}$$

where ω_{0i} = the center of region in which the lines are identified by the subscript i and ω_{0j} = the center of region in which the lines are identified by the subscript j. Since the temperature-dependent function $\varphi(T)$ is easily calculated theoretically, Eq. (23) may be used as the basic expression for the determination of population temperatures with high time resolution on a discrete line spectrum such as that of the (0, 0)-band of OH.

Application of an obvious extension of the proposed technique, using numerous detecting channels, should permit direct studies on the nature of the relaxation processes producing equilibration with respect to population distributions behind shock fronts. Measurements of this sort are of considerable theoretical interest.

EXPERIMENTAL DETERMINATION OF TRANSLATIONAL TEMPERATURE

Gaydon and Wolfhard[18] first performed direct measurements of spectral line profiles with very high resolution in order to determine translational temperatures. They assumed that the spectral absorption coefficients $P_{\,|\,\omega-\omega_0\,|}$ corresponded to a pure Doppler shape, *viz.*,

$$P_{\,|\,\omega-\omega_0\,|} = \frac{S}{\omega_0}\left(\frac{mc^2}{2\pi kT}\right)^{1/2} \cdot\left[\exp - \frac{(\omega - \omega_0)^2}{\omega_0^2}\frac{mc^2}{2kT}\right] \tag{24}$$

where S is the integrated intensity of the line under study whose center is located at the wave number ω_0, m is the mass of the emitter, c is the velocity of light, and the other symbols have their usual meaning. It is apparent from Eq. (24) that $P_{|\omega-\omega_0|}/(S/\omega_0)$ is a unique function of T and, furthermore, examination of the origin of Eq. (24) shows that the temperature involved is the translational temperature. Actually, T can also be obtained from a measurement of the half-width b_D of the spectral line, provided pure Doppler broadening obtains. Thus

$$b_D = \left(\frac{2kT}{mc^2}\right)^{1/2} \sqrt{\ln 2}\,\omega_0 \tag{25}$$

Except under special conditions at very low

pressures, spectral lines exhibit a variety of complicated broadening effects. Perhaps the best understood and most important effects at moderate temperatures of the line broadening phenomena involve the simultaneous occurrence of Doppler and collision broadening, in which case Eq. (24) is replaced by the expression

$$P_{|\xi|} = P'\left(\frac{a}{\pi}\right)\int_{-\infty}^{\infty}\frac{\exp(-y^2)}{a^2+(\xi-y)^2}\,dy \qquad (26)$$

where

$$P' = \frac{S}{\omega_0}\left(\frac{mc^2}{2\pi kT}\right)^{1/2}$$

$$a = \frac{(b_N + b_C)(\ln 2)^{1/2}}{b_D}$$

and

$$\xi = \frac{\omega-\omega_0}{\omega_0}\left(\frac{mc^2}{2kT}\right)^{1/2}$$

The parameter a depends on the ratio of the sum of the natural half-width b_N and the collision half-width b_C to b_D. Equations (24) and (25) apply exactly only for $a = 0$ and, in good approximation, only for a $\lesssim 10^{-4}$ for a wide range of optical depths.

Gaydon and Wolfhard[18] concluded from their studies on CH in C_2H_2-O_2 flames that excessive (i.e., greater than equilibrium) translational temperatures were present. This conclusion is, however, at variance with later and apparently more definitive studies[19, 20] in which the authors concluded that the apparent deviations from equilibrium temperature should actually be ascribed to the fact that collision broadening was not negligibly small and that, therefore, Eq. (26) rather than Eq. (25) should have been used for the interpretation of experimental data.

There does not appear to be any early prospect for the development of rapid high-resolution spectroscopic facilities suitable for the study of spectral line shapes, for example, in the emission spectra behind shock fronts. However, in systems of this sort, the direct determination of translational relaxation times is of considerable interest. For this reason, it is perhaps worthwhile to note that, under the unlikely conditions that the spectral line shape is accurately known or else may be approximated by a pure Doppler contour, a direct measurement of total line radiancy R_L may be used for a determination of translational temperatures directly behind the shock front. For pure Doppler broadening, it is easily shown[21] that

$$\frac{R_L}{R^0_{\omega_0\omega_0}} = \sum_{n=1}^{\infty} -\frac{1}{n!\sqrt{n}}\left(-\frac{SX}{\omega_0}\right)^n\left(\frac{mc^2}{2\pi kT}\right)^{(n-1)/2} \qquad (27)$$

where $R^0_{\omega_0}$ is the blackbody radiancy at the line center ω_0, X is the optical depth of the emitter, and the other symbols have the same meaning as in Eq. (26). But

$$\frac{SX}{\omega_0} = \frac{\pi e^2}{mc^2\omega_0} f(1 - e^{-hc\omega_0/kT_{\text{pop}}})N_l l$$

where l is the geometric length throughout which the emitters are distributed uniformly, f is the (constant) oscillator strength of the line, and N_l is the number of atoms or molecules per unit volume in the lower state with energy E_l of the transition producing the spectral line at ω_0. Thus

$$N_l = \frac{g_l(p/R)\exp(-E_l/kT_{\text{pop}})}{TQ_{T_{\text{pop}}}}$$

where g_l is the statistical weight of the lower state, p denotes the pressure of the emitter, R is the appropriate gas constant, and $Q_{T_{\text{pop}}}$ is the total partition function evaluated at a population temperature T_{pop}. For optical depths that are so small that only the first term needs to be included in Eq. (27), we find that

$$R_L = \left(\frac{2\pi^2e^2h\omega_0{}^3p}{mR}fl\right)\frac{\exp(-hc\omega_0/kT_{\text{pop}})}{T}\cdot\left[\frac{g_l\exp(-E_l/kT_{\text{pop}})}{Q_{T_{\text{pop}}}}\right] \text{ for } SX \text{ sufficiently small} \qquad (28)$$

Consider now a process in which translational relaxation (i.e., adjustment of T) occurs prior to any changes in population temperature (T_{pop}). In this case, it is apparent from Eq. (28) that the rate of change of $\ln R_L$ with time,

$$\frac{\partial \ln R_L}{\partial t} = -\frac{1}{T}\frac{\partial T}{\partial t} \qquad (29)$$

is directly related to the rate of change of translational temperature with time. The absolute value of T as a function of time, for constant and known values of $g_l\exp(-E_l/kT_{\text{pop}})/Q_{T_{\text{pop}}}$, may be calculated from Eq. (28) provided absolute measurements have been made of R_L as a function of time for transparent gases with known f number at sufficiently low pressures to justify the assumption that we are dealing with practically pure Doppler broadening. The nature of the relaxation process involving population tem-

peratures requires independent study (compare the section on Measurement of Population Temperatures). A suitable experimental procedure for measuring R_L directly with high time resolution is essentially equivalent to the technique described in the section on Measurement of Population Temperatures.

TEMPERATURE MEASUREMENTS IN NONISOTHERMAL SYSTEMS WITH "LOCAL EQUILIBRIUM" AND AXIAL SYMMETRY[11]

Consider an emitting region with circular cross section of radius R (see Fig. 7). The origin of a rectangular coordinate system coincides with the center of the emitting region. The spectrally emitted steradiancy coming from a line parallel to the y axis and located at x is then given by the relation

$$B_{\lambda,x} = \frac{1}{\pi} \int_{-\sqrt{R^2-x^2}}^{\sqrt{R^2-x^2}} R^0_{\lambda,r} P_{\lambda,r} p_r \, dy \cdot \exp\left[-\int_y^{\sqrt{R^2-x^2}} P_{\lambda,r} p_r \, dy' \right] \tag{30}$$

where $R^0_{\lambda,r}$ is the spectrally emitted blackbody radiancy at the radial distance r, $P_{\lambda,r}$ is the spectral absorption coefficient (in cm^{-2}-$atmos^{-1}$) at r, and p_r is the corresponding partial pressure of the emitting species (in atmospheres); thus $P_{\lambda,r} p_r = k_{\lambda,r}$ is the linear absorption coefficient (in cm^{-1}) in the wavelength interval between λ and $\lambda + d\lambda$ at the radial distance r. If a real image can be reflected of the line source on itself (for example, by using a long focal length spherical mirror for emitting regions with large temperature gradients, or by using a plane mirror and good collimation for emitting regions with small temperature gradients) with steradiancy $\alpha_\lambda B_{\lambda,x}$, then the observable spectral steradiancy for the double-path experiment is

$$B^D_{\lambda,x} = B_{\lambda,x} + \alpha_\lambda B_{\lambda,x} \exp\left[-\int_{-\sqrt{R^2-x^2}}^{\sqrt{R^2-x^2}} k_{\lambda,r} \, dy' \right] \tag{31}$$

Since the parameters $B_{\lambda,x}$, α_λ and $B^D_{\lambda,x}$ can presumably be measured directly, it is convenient to rewrite Eq. (31) in the form

$$-\ln \frac{1}{\alpha_\lambda} \left(\frac{B^D_{\lambda,x}}{B_{\lambda,x}} - 1 \right) = 2 \int_0^{\sqrt{R^2-x^2}} k_{\lambda,r} \, dy' \tag{32}$$

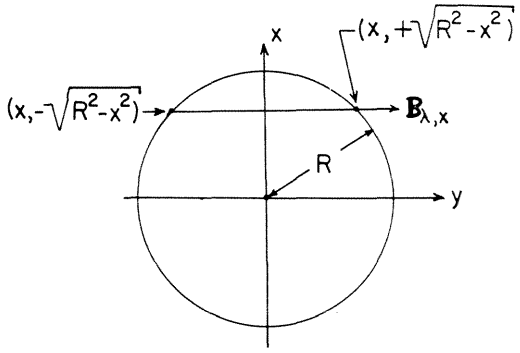

FIG. 7. Schematic diagram identifying the coordinates used in the analysis of an axially symmetric emitting region.

where we have taken advantage of the fact that $k_{\lambda,r}$ must be an even function of the coordinate y'. A change of variables transforms Eq. (32) into Abel's integral equation[22] which may be solved with the result

$$k_{\lambda,r} = -\frac{1}{\pi r} \frac{d}{dr} \int_r^R \left[-\ln \frac{1}{\alpha_\lambda} \left(\frac{B^D_{\lambda,x}}{B_{\lambda,x}} - 1 \right) \right] \cdot \frac{x \, dx}{\sqrt{x^2 - r^2}} \tag{33}$$

In this manner the linear spectral absorption coefficient may be determined as a function of r for $0 \leq r \leq R$. The experimental precision depends on the extent of self-absorption and must become very low for $k_{\lambda,r}$ so large that the ratio $B^D_{\lambda,x}/B_{\lambda,x}$ is not appreciably greater than unity or else approaches two.

The schematic arrangement sketched in Figs. 1 or 2 can clearly be adapted for measurements of $k_{\lambda,r}$ with short time response on axially symmetric systems.

For a given emitting species it is, of course, possible to relate $k_{\lambda,r}$ uniquely to the local temperature provided the system is locally in equilibrium. Hence a measurement of $k_{\lambda,r}$ is equivalent to a determination of T_r. In practice, it may be necessary to perform either elaborate theoretical calculations or else elaborate auxiliary measurements in order to obtain $k_{\lambda,r}$ as a function of the temperature.

Various special solutions of Eq. (33) have been considered by Freeman and Katz[11] to whom we refer for further discussions concerning the application of Eq. (33) and also for representative experimental results obtained on a plasma jet. The final conversion of measured data of $k_{\lambda,r}$ to T_r has not yet been described (see, however, the following section).

TEMPERATURE MEASUREMENTS IN IONIZED GASES

A survey of techniques suitable for temperature measurements in ionized gases has been prepared recently by Lochte-Holtgreven.[4] We shall content ourselves here with amplifying this survey by emphasizing the fact that the equilibrium values of the spectral absorption coefficients can be calculated as a function of the temperature.

The theoretical expression for the continuum absorption coefficient (in cm^2/g of neutral H) associated with bound-free and free-free transitions in a hydrogen plasma, produced only by processes involving the neutral atoms, is given by the expression

$$k_{c,\nu} = \frac{32}{3\sqrt{3}} \frac{\pi^2 e^6 R_Y}{h^3 m_H} \frac{1 - \exp(-h\nu/kT)}{\nu^3} \cdot \exp(-x_1) \left[\sum_{\nu_n < \nu}^{\infty} \frac{\exp(x_n)}{n^3} \bar{g}_{G,bf} + \frac{\bar{g}_{G,ff}}{2x_1} \right] \tag{34}$$

where R_Y is the Rydberg constant, m_H is the mass of the hydrogen atom,

$$x_n = \frac{hcR_Y}{kTn^2} = \frac{x_1}{n^2} \quad ,$$

the Gaunt factors for bound-free transitions ($\bar{g}_{G,bf}$) range[23] from 0.90 to 1.10 whence the approximation $\bar{g}_{G,bf} \simeq 1$ may be used, and the Gaunt factors for free-free transitions ($\bar{g}_{G,ff}$) have been studied by Greene[24] and extrapolated by Olfe[25] to lower temperatures with the recommended value being $\bar{g}_{G,ff} \simeq 1.24$ for $T \lesssim 10{,}000°K$. In the sum of Eq. (34) we must include all terms for which the frequency ν exceeds the frequency ν_n required for a bound-free transition. A plot giving $(k_{c,\omega})_H/p_H$ as a function of ω and temperature is shown in Fig. 8. Reference to Fig. 8 shows that an experimental measurement of $k_{c,\omega}$ is equivalent to a temperature determination under conditions in which the hydrogen atoms are practically unionized.

Actually, the continuum absorption coefficient in a hydrogen plasma depends on many processes other than those that have been allowed for in constructing Fig. 8. For an exhaustive discussion of this problem we refer to Olfe.[25] In Fig. 9 we

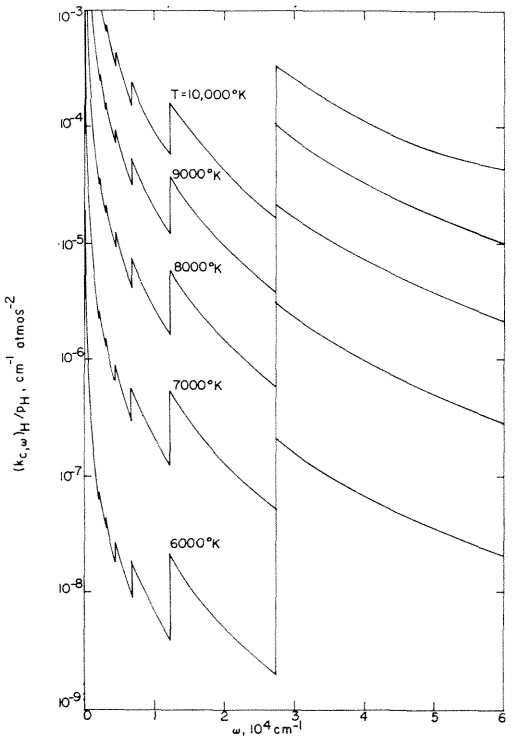

FIG. 8. The absorption coefficient term $(k_{c,\omega})_H/p_H$ at various temperatures (reproduced from reference 25).

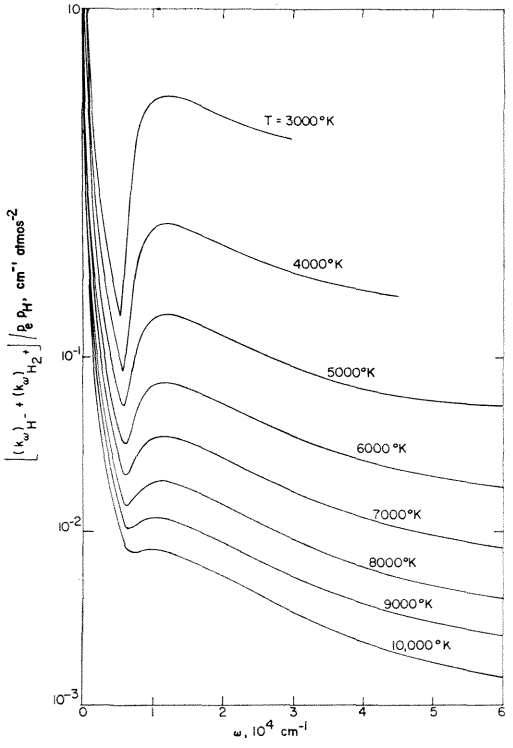

FIG. 9. The absorption coefficient term $[(k_\omega)_H + (k_\omega)_{H_2^+}]/p_A p_H$ at various temperatures (reproduced from reference 25).

have reproduced his results for the equilibrium value of

$$[(k_\omega)_{H^-} + (k_\omega)_{H_2^+}]/p_e p_H$$

as a function of ω and T.[25] It is apparent that information of the type plotted in Figs. 8 and 9 is sufficient for an unambiguous determination of equilibrium temperatures in a hydrogen plasma from experimental measurements of absorption coefficients. This information may also be used in conjunction with measurements of the type discussed in the section on Temperature Measurements in Nonisothermal Systems with "Local Equilibrium" and Axial Symmetry for reconstructing temperature profiles in hydrogen plasmas with axial symmetry, provided the assumption that local equilibrium obtains is justified.

The theoretical calculation of plots similar to those shown in Figs. 8 and 9, for plasmas other than a hydrogen plasma, should clearly be of value in the interpretation of spectroscopic investigations on plasma radiation.

TEMPERATURE MEASUREMENTS OF THE HEATED SHOCK LAYER IN FRONT OF CONICAL REENTRY BODIES AND CONICAL HYPERVELOCITY BALLISTIC PELLETS[26]

Theoretical calculations concerning the aerodynamic flow over conical bodies moving at high velocity suggest that the gas volume between the shock front and the cone surface may be considered to be isothermal in first approximation. Furthermore, using available emissivity estimates for heated air, it is known that the transparent gas approximation may be used for the heated gas volume.

For observations at distances from the source that are large compared with the physical dimensions of the source, the total radiant energy flux E_d received by a detector is easily shown to be given by the relation

$$E_d = \left(\lim_{x\to 0} \frac{d\epsilon}{dx}\right) \sigma T^4 \frac{V}{\pi} \frac{A_d}{R^2} \tag{35}$$

where

$$\left(\lim_{x\to 0} \frac{d\epsilon}{dx}\right)$$

is the total hemispherical emissivity of the heated gases in the shock layer to the transparent gas approximation, V is the volume of the emitting gases which are assumed to be at the uniform temperature T, A_d is the detector area which is aligned in a direction normal to the distance R between the detector and the emitting gases. Consider the emitting volume sketched in Fig. 10. The gas volume is evidently given by the relation

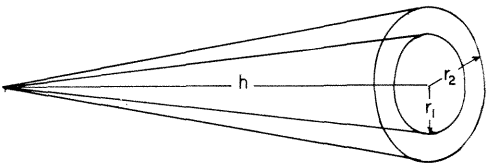

FIG. 10. Schematic diagram of the emitting volume formed over a hypervelocity conical body.

$$V = \frac{\pi}{3} (r_2^2 - r_1^2)h$$

It follows now from Eq. (35) that, in the absence of the solid body,

$$E_d = \left(\lim_{x\to 0} \frac{d\epsilon}{dx}\right) \sigma T^4 \left[\frac{1}{3} (r_2^2 - r_1^2)h\right] \frac{A_d}{R^2} \tag{36}$$

If the solid body does not emit, observations are made of either the upper or the lower half of the gas volume, and the solid body provides "reverse spectral reflection" of the incident radiation, Eq. (36) must still hold. On the other hand, if the solid body absorbs all of the incident radiant energy, observations are made of either the upper or lower gas volume, and if the solid body does not emit, then the expression given for E_d in Eq. (36) must be multiplied by $\frac{1}{2}$ in order to obtain the received radiant energy flux.

Let the reflectivity of the solid body be r_b and its emissivity ϵ_b at the temperature T_b; then the total radiant energy flux E incident on the detector viewing the entire gas volume and solid surface is

$$E = (1 + r_b)E_d + \epsilon_b \sigma T_b^4 \frac{r_1^2 A_d}{R^2}$$

or

$$E = \frac{A_d}{R^2} \left\{ (1 + r_b) \left(\lim_{x\to 0} \frac{d\epsilon}{dx}\right) \cdot \left[\frac{1}{3} (r_2^2 - r_1^2)h\right] \sigma T^4 + \epsilon_b \sigma T_b^4 r_1^2 \right\} \tag{37}$$

Here we have again assumed that reverse spectral reflection occurs from the solid body.

It is apparent from Eq. (37) that a direct meas-

urement of E and T_b determines T since

$$\left(\lim_{x\to 0}\frac{d\epsilon}{dx}\right)$$

is known as a unique function of T from independent emissivity measurements or calculations on heated air.[27, 28]

For spectrally resolved measurements in the wavelength interval $\Delta\lambda$ between λ_1 and λ_2, Eq. (37) should be replaced by the expression

$$E_{\Delta\lambda} = \left\{\frac{A_d}{R^2}\left[\frac{1}{3}(r_2^2 - r_1^2)h\right]\int_{\lambda_1}^{\lambda_2}(1 + r_{b,\lambda}) \cdot\left(\lim_{x\to 0}\frac{d\epsilon}{dx}\right)_\lambda [R_\lambda^0(T)]\, d\lambda + r_1^2\int_{\lambda_1}^{\lambda_2}\epsilon_{b,\lambda}[R_\lambda^0(T_b)]\, d\lambda\right\} \tag{37a}$$

where the subscript λ identifies appropriate spectral quantities, and $R^0(T)$ and $R^0(T_b)$ denote, respectively, the spectral blackbody radiancies evaluated at the gas temperature (T) and at the surface temperature of the body (T_b).

For experimental studies in which the detector is located in such a way that the cone is observed at a large distance R from the cone axis, in a direction normal to the cone axis, the contribution to the radiant flux from the solid surface becomes

$$\frac{1}{\pi}\epsilon_b\sigma T_b^4 r_1 h\,\frac{A_d}{R^2}$$

At the same time, a portion of the gas volume is now shielded by the solid body in such a way that of the total gas volume only the fraction

$$1 - \xi$$

is observed. Here

$$\xi = \frac{1}{2} + \frac{1}{\pi(r_2^2 - r_1^2)} \cdot\left[r_1\sqrt{r_2^2 - r_1^2} - r_2^2\sin^{-1}\left(\frac{\sqrt{r_2^2 - r_1^2}}{r_2}\right)\right]$$

and

$$\lim_{r_2\to r_1}\xi = \frac{1}{2}, \qquad \lim_{r_2\to\infty}\xi = 0.$$

Thus Eq. (37) should be replaced by the expression

$$E = \frac{A_d}{R^2}\left\{(1 + r_b)\left(\lim_{x\to 0}\frac{d\epsilon}{dx}\right) \cdot\left[\frac{1}{3}(r_2^2 - r_1^2)h\right]\sigma T^4(1 - \xi) + \frac{1}{\pi}\epsilon_b\sigma T_b^4 r_1 h\right\}$$

Other obvious modifications of the basic relations are easily derived for observations of selected fractions of the radiating gas volume.

PRECISION TEMPERATURE MEASUREMENTS FROM THE DETERMINATION OF THRESHOLDS FOR MASER-TYPE OPERATION OF INFRARED CELLS

An iraser detector utilizing the experimental arrangement sketched in Fig. 11 has been described recently.[29] The device consists essentially of a highly reflecting cylinder with elliptical cross section at the foci of which are centered two long cylindrical tubes containing the same diatomic gas. One of the tubes contains the gas at low temperature (T_0) and low pressure, whereas the other tube contains gas at an elevated temperature (T_g). Tube materials and pressures are to be chosen in such a way that, at the steady state, (a) the rotational population distribution of the cold gas is equilibrated at the translational temperature of the tube, (b) surface deactivation of vibrationally excited species is unimportant, and (c) the radiative life times of the vibrationally excited emitters are short compared with the time required for vibrational deactivation by gas-phase collisions. The specified conditions can apparently be satisfied for such gases as HCl and HF.[29]

A straightforward analysis, using procedures similar to those usually employed in maser studies,[30–35] shows, for example, that

$$\frac{N_{7,1}}{N_{8,0}} \simeq \frac{(15/17)\exp(30hcB_e/kT_0) + (15/17)(8/7)}{[\exp(hc\omega_e/kT_g)][1 + (8/7)]} \tag{38}$$

at the steady state if $N_{n,j}$ denotes the number of molecules per unit volume in the nth vibrational and in the jth rotational level.

It is apparent from Eq. (38) that the steady-state value of the ratio $N_{7,1}/N_{8,0}$ is a sensitive function of T_0 and T_g. Hence the resonance condition for maser-type operation may be used for a precision determination of either T_0 or T_g. In practice, measurements of this type are probably mostly of interest for sources at high tem-

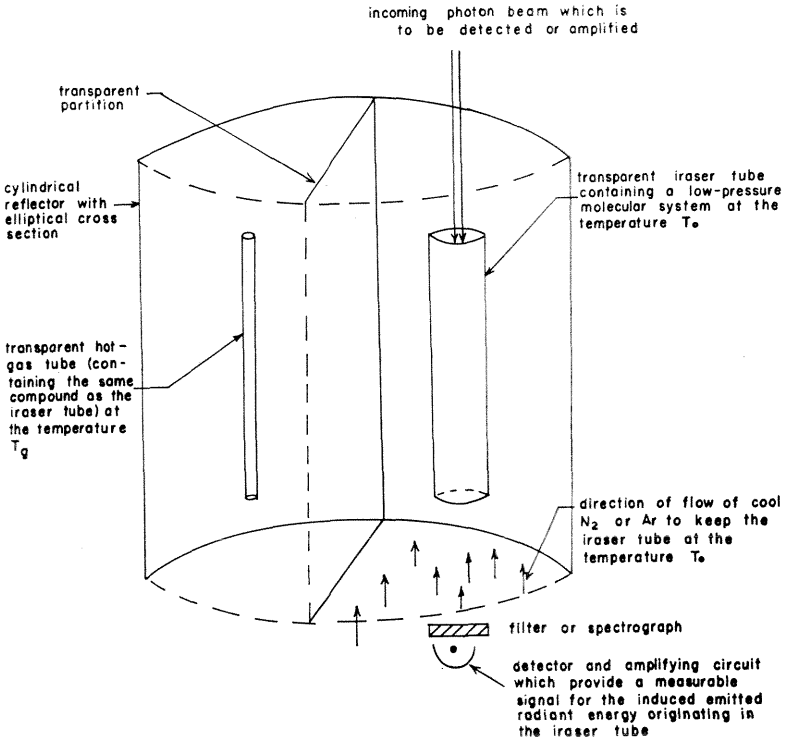

FIG. 11. Schematic diagram of an iraser detector or coherent infrared light source.

peratures T_g. Unfortunately, the proposed method of measurement is feasible only for systems for which such population ratios as $N_{7,1}/N_{8,0}$ may be made larger than unity, i.e., for molecules with relatively large values of B_e. For HCl we find, for example, that $(N_{7,1}/N_{8,0})_{\mathrm{HCl}} \simeq 2.19$ for $T_0 = 300°\mathrm{K}$ and $T_g = 3000°\mathrm{K}$. Hence it follows that the system sketched in Fig. 11 might be used for temperature measurements on gases containing HCl at several thousand degrees Kelvin. A similar statement applies also to temperature measurements through threshold determinations for maser-type operation of HF. These measurements may be of practical interest in connection with performance and reaction rate studies on rocket gases containing fluorine, hydrogen, and chlorine. However, the prime application, if any, of the iraser resonance condition will probably be for determining reference temperatures with high precision in the 2500 to 3000°K range.

References

1. *Temperature, Its Measurement and Control in Science and Industry*, (Reinhold Publishing Corporation, New York, 1941), Vol. 1, Chaps. 8 and 12.
2. *Temperature, Its Measurement and Control in Science and Industry*, (Reinhold Publishing Corporation, New York, 1955), Vol. 2, Chaps. 3, 4, 15, and 17.
3. S. S. Penner, *Quantitative Molecular Spectroscopy and Gas Emissivities*, (Addison-Wesley Publishing Company, Reading, Massachusetts, 1959), Chaps. 16 and 17.
4. W. Lochte-Holtgreven, Repts. on Progr. Phys. **21**, 312-383 (1958).
5. A. G. Gaydon and H. G. Wolfhard, *Flames, Their Structure, Radiation, and Temperature* (Chapman and Hall, London, 1960), second edition.
6. J. G. Clouston, A. G. Gaydon, and I. I. Glass, Proc. Roy. Soc. (London) **248A**,, 429 (1958).
7. J. G. Clouston, A. G. Gaydon, and I. R. Hurle, Proc. Roy. Soc. (London) **252A**, 143 (1959).
8. S. S. Penner, E. N. Bennett, F. Harshbarger, and W. J. Hooker, *Shock Tubes*, edited by A. Ferri (Pergamon Press, Ltd., London, 1961), Chap. IV E.
9. H. E. Petschek, P. H. Rose, H. S. Glick, A. Kane, and A. Kantrowitz, J. Appl. Phys. **26**, 83 (1955).

10. E. B. Turner, *NSF Conference on Stellar Atmospheres*, Indiana University, Bloomington, 1954, pp. 52–61.
11. M. P. Freeman and S. Katz, J. Opt. Soc. Am. **50,** 826 (1960); see also R. W. Larenz, Z. Physik **129,** 327 (1951).
12. S. Silverman, *Third International Combustion Symposium* (Williams and Wilkins Company, Baltimore, 1959), pp. 498–500.
13. W. J. Hooker, M. Lapp, D. Weber, and S. S. Penner, J. Chem. Phys. **25,** 1087 (1956).
14. Reference 3, Chap. 12.
15. S. S. Penner, D. B. Olfe, and J. A. L. Thomson, *Thermodynamic and Transport Properties of Gases, Liquids, and Solids* (McGraw-Hill Book Company, Inc., New York, 1959), pp. 2–13.
16. U. P. Oppenheim, J. Appl. Phys. **30,** 803 (1959).
17. M. Lapp, J. Quant. Spectros. & Rad. Transfer, **1, 30** (1961); see also S. S. Penner, D. B. Olfe, and M. Lapp, *Symposium on Heat Transfer* (American Society of Mechanical Engineers, New York, 1961).
18. A. G. Gaydon and H. G. Wolfhard, Proc. Roy. Soc. (London) **199A,** 89 (1949).
19. B. W. Harned and N. Ginsburg, J. Opt Soc. Am. **48,** 178 (1958).
20. D. H. Rank, G. Saksena, and T. A. Wiggins, J. Opt. Soc. Am. **48,** 521 (1958).
21. Reference 3, p. 39.
22. E. C. Titchmarsh, *Introduction to the Theory of Fourier Integrals*, (Oxford University Press, Oxford, 1948), second edition, p. 331.
23. H. Mayer, Los Alamos Scientific Laboratory Rept. LA-647, Los Alamos, 1947.
24. J. Greene, Astrophys. J. **130,** 693 (1959).
25. D. B. Olfe, J. Quant. Spectros. & Rad. Transfer, **1, 104** (1961).
26. D. B. Olfe and S. S. Penner, "Total and Spectral Emissivity Measurements on Conical Reentry Bodies and Conical Hypervelocity Ballistic Pellets," Report ZPh-067, Physics Section, Convair, San Diego, California (September, 1960).
27. B. Kivel and K. Bailey, AVCO Research Rept. No. 21, Everett, Mass., 1957.
28. Reference 3, Chapt. 14.
29. S. S. Penner, "On Iraser Detectors for Radiation Emitted from Diatomic Gases and Coherent Infrared Sources," Report of the Physics Section, Convair, San Diego, California (January, 1961), see also J. Quant. Spectros. & Rad. Transfer, **1,** 163 (1961).
30. J. R. Singer, *Masers* (John Wiley & Sons, Inc., New York, 1959).
31. A. L. Schawlow and C. H. Townes, Phys. Rev. **112,** 1940 (1958).
32. A. M. Prokhorov, J. Exptl. Theoret. Phys. **34,** 1658 (1958).
33. R. H. Dicke, U. S. Patent No. 2,851,652 (September 9, 1958).
34. *Quantum Electronics—A Symposium*, edited by C. H. Townes (Columbia University Press, New York, 1960).
35. N. Bloembergen, Phys. Rev. **104,** 324 (1956).